AGU PUBLICATIONS

Journal of Advances in Modeling Earth Systems

RESEARCH ARTICLE
10.1002/2015MS000578

This article is a companion to *Li et al.* [2016], doi:10.1002/2015MS000579.

Key Points:
- An urban canopy model is developed
- The model is suitable for climate and earth system simulations
- The model is validated

Correspondence to:
D. Li,
lidan@bu.edu

Citation:
Li, D., S. Malyshev, and E. Shevliakova (2016), Exploring historical and future urban climate in the Earth System Modeling framework: 1. Model development and evaluation, *J. Adv. Model. Earth Syst.*, *8*, 917–935, doi:10.1002/2015MS000578.

Received 29 OCT 2015
Accepted 11 MAY 2016
Accepted article online 17 MAY 2016
Published online 12 JUN 2016

Exploring historical and future urban climate in the Earth System Modeling framework: 1. Model development and evaluation

Dan Li[1,2], Sergey Malyshev[3], and Elena Shevliakova[4]

[1]Program of Atmospheric and Oceanic Sciences, Princeton University, Princeton, New Jersey, USA, [2]Department of Earth and Environment, Boston University, Boston, Massachusetts, USA, [3]Department of Ecology and Evolutionary Biology, Princeton University, Princeton, New Jersey, USA, [4]Geophysical Fluid Dynamics Laboratory, Princeton, New Jersey, USA

Abstract A number of recent studies investigated impacts of Land-Use and Land-Cover Changes (LULCC) on climate with global Earth System Models (ESMs). Yet many ESMs are still missing a representation of the most extreme form of natural landscape modification – urban settlements. Moreover, long-term (i.e., decades to century) transitions between build-up and other land cover types due to urbanization and de-urbanization have not been examined in the literature. In this study we evaluate a new urban canopy model (UCM) that characterizes urban physical and biogeochemical processes within the subgrid tiling framework of the Geophysical Fluid Dynamics Laboratory (GFDL) land model, LM3. The new model LM3-UCM is based on the urban canyon concept and simulates exchange of energy, water (liquid and solid), and carbon between urban land and the atmosphere. LM3-UCM has several unique features, including explicit treatment of vegetation inside the urban canyon and dynamic transition between urban, agricultural and unmanaged tiles. The model is evaluated using observational data sets collected at three urban sites: Marseille in France, Basel in Switzerland and Baltimore in the United States. It is found that LM3-UCM satisfactorily reproduces canyon air temperature, surface temperatures, radiative fluxes, and turbulent heat fluxes at the three urban sites. LM3-UCM can capture urban features in a computationally efficient manner and is incorporated into the land component of GFDL ESMs. This new capability will enable improved understanding of climate change effects on cities and the impacts of urbanization on climate.

1. Introduction

Land-Use and Land-Cover Changes (LULCC) at local, regional and global scales have been shown to play an important role in modulating the Earth's climate, its hydrological and biogeochemical cycles [*Findell et al.*, 2007; *Mahmood et al.*, 2014; *Malyshev et al.*, 2015; *Pielke et al.*, 2011]. Urbanization is an extreme case of LULCC through which natural landscapes are turned into man-made landscapes. Urbanization alters surface aerodynamic, thermodynamic and hydrologic properties, which concomitantly change surface turbulent and energy fluxes and, as a result, surface/near-surface temperatures [*Arnfield*, 2003; *Oke*, 1982] as well as precipitation [*Li et al.*, 2013; *Niyogi et al.*, 2011; *Shepherd*, 2005]. Buildings and other man-made structures in urban areas also affect the turbulent flow and transport at local, neighborhood and city scales [*Bou-Zeid et al.*, 2009; *Wang et al.*, 2014; *Wood et al.*, 2010; *Yu et al.*, 2013]. Urban areas are important sources of greenhouse gas emissions as well as anthropogenic heat and aerosol emissions [*Grimmond*, 2007]. Therefore, quantifying the impacts of urbanization on the climate system at various temporal and spatial scales is important for proper representation of land-atmosphere interactions, and has been the subject of active research. Of equal importance is to quantify the impacts of global climate change on urban areas, where more than 50% of the world's population live, and to assess urban mitigation and adaption strategies [*Li et al.*, 2014]. Due to the many unique features of urban areas, it is expected that urban areas will respond in a different way to the global climate change as compared to rural areas [*Fischer et al.*, 2012; *Li and Bou-Zeid*, 2013; *Li et al.*, 2015; *McCarthy et al.*, 2010; *Oleson*, 2012].

In order to examine the impacts of urbanization on the climate system and the impacts of global climate change on urban areas, it is important to integrate urban representations into Global Climate Models (GCMs) and Earth System Models (ESMs). There have been continuous efforts toward this goal and

numerous urban parameterizations, with different levels of complexity, have been proposed. *Masson* [2006] classified urban parameterizations into three main categories: 1) empirical models that are based on statistical fitting to observations, 2) modified land surface models (LSMs), originally designed for natural vegetated or bare surfaces and later adapted to represent urban landscapes, and 3) urban canopy models (UCMs). Empirical models that calculate fluxes based on statistical fitting to observations (e.g., assuming that the ground heat flux is a fixed fraction of the net radiation) are usually limited to areas where the observations were taken. Traditional LSMs, even with modified parameters for urban surfaces (e.g., albedo, emissivity, heat capacity, thermal conductivity, and roughness length), have been shown to be still inadequate to capture urban fluxes [*Grimmond et al*., 2010, 2011] and the urban heat island effect [*Lee et al*., 2011; *Zhang et al*., 2011]. Because UCMs better represent unique urban characteristics (e.g., multiple reflections of radiation among buildings), they are receiving more attention even though they usually require a large number of inputs.

The international urban energy balance model comparison project [*Grimmond et al*., 2010., 2011] systematically compared and evaluated 32 urban parameterization schemes and found that the models generally do well in simulating radiation exchanges but have strong biases in simulating latent heat fluxes. The more complex schemes such as UCMs have more potential for improvements as compared to simpler models whose performance is more dependent on parameter calibration. *Grimmond et al* [2010, 2011] also concluded that taking vegetation into account is important, and integrating vegetation into the urban scheme better captures urban fluxes as compared to treating vegetation separately.

Motivated by the need to better understand both the impacts of global climate change in urban areas and the feedbacks of urbanization on climate, we develop an UCM in the subgrid tiling framework of GFDL land model LM3 [*Milly et al*., 2014; *Shevliakova et al*., 2009], which provides surface boundary conditions to the atmosphere. Increasing attention has been given to land models' capabilities, enabling improved understanding of the interactions among the hydrological cycle, biophysical and biogeochemical processes, as well as human activities. This is particularly important when land models are used in ESMs to assess effects of LULCC [*Lawrence et al*., 2012]. While urban areas account for a small fraction of global land, the resolution of ESMs is increasing and the urban sprawl is continuing. Therefore, it is critical to develop a detailed representation of urban processes for supporting model-based investigations of urban climate, hydrological and biogeochemical cycles, which is essential for designing sustainability-related strategies and policies for regions with large population densities.

The aim of this paper, which is the first part of a series toward exploring historical and future urban climate within GFDL's Earth System Modeling framework, is to describe a new UCM and to evaluate its performance using offline simulations (i.e., land model simulations driven by observational data sets rather than coupled with a free-running atmospheric model). We also compare our UCM to other UCMs in terms of model structure and performance. The paper is organized as follows: Section 2 describes the model structure. Section 3 presents the comparison between simulated results at three urban sites and observations. Section 4 concludes the paper.

2. Model Description

2.1. Model Requirements

In a GCM or an ESM, a land model has to provide bottom boundary conditions for the atmospheric model, with fields such as radiative and turbulent fluxes. Within the GFDL flexible modeling framework [*Balaji et al*., 2006], LM3 represents each grid-cell's surface heterogeneity as a collection of tiles [*Milly et al*., 2014; *Shevliakova et al*., 2009]. Each tile has its own energy and water balances throughout the vegetation-soil column and its own exchange coefficients with the atmosphere. Contributions of each tile are aggregated at the bottom atmospheric layer so that the atmosphere only feels the area-averaged fluxes [*Balaji et al*., 2006]. The primary goal of our study is to introduce an UCM that handles an urban tile in LM3 (hereafter called LM3-UCM).

A unique requirement associated with developing an urban parameterization for decadal to century scale climate or ESM simulations is that the location and size of the urban area must be dynamic in order to represent transitions from rural land to urban land and vice versa. Allowing urban area to change is also critical for assessing the historical and future hydroclimatic impacts of urban expansions, which is one of the overarching goals of our study. This dynamic feature makes our urban implementation different from most

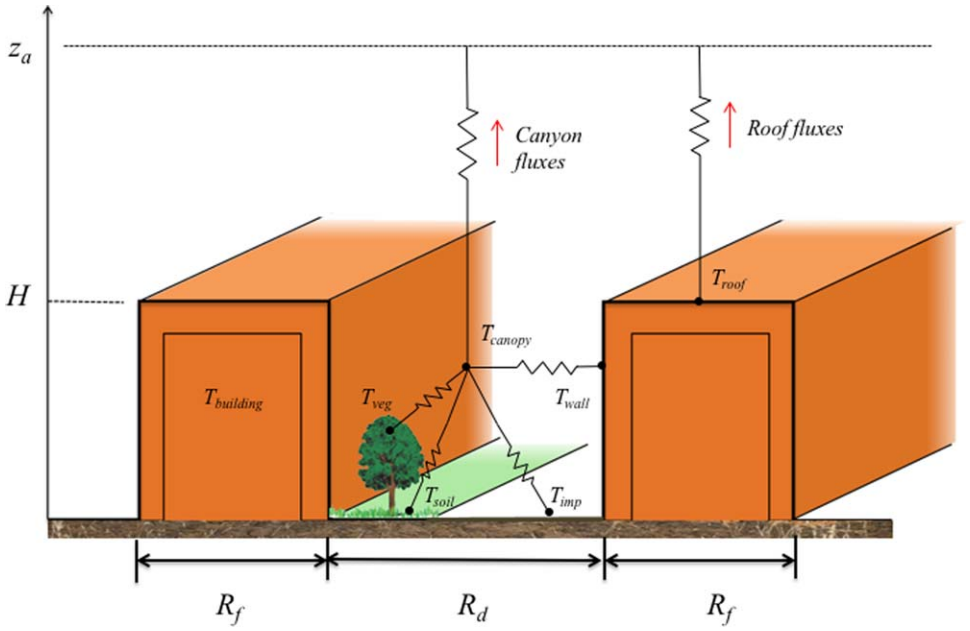

Figure 1. A schematic of the LM3 urban canopy model. z_a is the height of the lowest level in the atmospheric model; H is the averaged height of buildings; R_f is the roof width and R_d is the canyon width. T_{roof} is the roof surface temperature; T_{wall} is the wall surface temperature; $T_{building}$ is the temperature of the building interior; T_{canopy} is the canopy air temperature within the urban canyon; T_{veg} is the vegetation temperature; T_{soil} is the soil surface temperature; T_{imp} is the impervious surface temperature.

other urban parameterizations such as the Community Land Model Urban (CLMU) [*Oleson et al*., 2008] as well as the single-layer urban canopy model (SLUCM) [*Kusaka et al*., 2001] in the Weather Research and Forecasting (WRF) model, since in these models urban tiles do not transition from/to other land-cover tiles and these models do not account for, for example, transfers of matter and energy during such transitions.

2.2. Model Structure

In light of the above requirements, we design LM3-UCM based on the urban canopy concept (see Figure 1), which is different from many urban parameterizations that do not explicitly consider the canopy structure [*Best et al*., 2006; *Jarvi et al*., 2011, 2014]. However, we do not model mass, momentum and energy exchanges at multiple levels within the canopy as compared to multi-layer UCMs [*Kondo et al*., 2005; *Martilli et al*., 2002]. The single layer LM3-UCM is composed of two major components: a roof component and a canyon component. These two components do not interact with each other directly; instead, they communicate with the bottom atmospheric layer through which they interact with each other. The canyon component includes the walls, the impervious surface at the ground, the pervious surface at the ground (i.e., soil), and the vegetation above soil. These are called subcomponents of the urban canyon hereafter. All of these four subcomponents communicate with the canopy air in the urban canyon, through which they interact with each other and also the atmosphere. The area fractions of pervious and impervious ground are denoted as f_P and f_{IMP} ($f_P + f_{IMP} = 1$), respectively. In this paper, we use "the pervious part of the ground" to indicate the combination of vegetation and soil, while "the impervious part of the ground" to indicate the impervious surface such as pavements. Soil underlies both pervious and impervious ground. Water, heat and carbon are exchanged between soil, vegetation and canopy air. Water and heat are also exchanged between impervious ground and canopy air, but the walls and canopy air only exchange sensible heat. In addition, heat is exchanged at the interface between soil and the impervious surface. The roof and walls also interact with the building interior through conductive heat fluxes but no interactions are allowed between buildings and soil.

LM3-UCM is different from the SLUCM in WRF [*Kusaka et al*., 2001] and the Town Energy Balance (TEB) model [*Masson*, 2000] in its explicit treatment of vegetation as an integral part of the urban canyon, instead of considering vegetation outside of the urban canyon as in SLUCM or TEB. However, it is noted that recent improvements have been made to incorporate vegetation into the urban canyon in the TEB model

[*Lemonsu et al*., 2012] and other single-layer UCMs [*Wang et al*., 2013]. Our model is conceptually similar to the CLMU with a few distinct features: first, vegetation is handled by a dynamic vegetation module [*Shevliakova et al*., 2009] here but is parameterized by a simplified bulk scheme in CLMU. In addition, the roof component of our model communicates with the atmospheric model directly while in CLMU the roof component interacts with the canopy air in the urban canyon, which essentially assumes that the air in the urban canyon and on the roof is well mixed. A recent study using CLMU found that this assumption results in higher roof temperature as compared to observations and decoupling the roof from the canyon is important [*Demuzere et al*., 2013].

2.3. Physical Parameterizations

2.3.1. Shortwave Radiation

At the roof surface, the total downward shortwave radiation flux is a combination of the direct (indicated by the subscript "*dir*") solar radiation ($S^{\Downarrow}_{dir}$, W m^{-2}) and the diffuse (indicated by the subscript "*dif*") solar radiation ($S^{\Downarrow}_{dif}$,W m^{-2}) from the atmosphere, so the net shortwave radiation (S_R, where the subscript "*R*" denotes roof) is

$$S_R=\left(1-\alpha_{R,dir}\right)S^{\Downarrow}_{dir}+\left(1-\alpha_{R,dif}\right)S^{\Downarrow}_{dif}, \tag{1}$$

where $\alpha_{R,dir}$ and $\alpha_{R,dif}$ are the roof albedos for direct and diffuse solar radiation, respectively. Within the urban canyon, radiative exchanges are parameterized following *Masson* [2000] for direct solar radiation and *Harman et al*. [2004] for diffuse solar radiation. Below we describe essential features of radiation exchange within the urban canyon.

First, sky view factors (F_s) of each subcomponent of the urban canyon are calculated following [*Harman et al*., 2004; *Wang et al*., 2013]:

$$\begin{aligned}
F_{GS}&=\sqrt{1+\left(\frac{H}{R_d}\right)^2}-\frac{H}{R_d}\\
F_{GW}&=\frac{1}{2}\left(1+\frac{H}{R_d}-\sqrt{1+\left(\frac{H}{R_d}\right)^2}\right)\\
F_{WW}&=\sqrt{1+\left(\frac{R_d}{H}\right)^2}-\frac{R_d}{H}\\
F_{WS}&=F_{WG}=\frac{1}{2}\left(1+\frac{R_d}{H}-\sqrt{1+\left(\frac{R_d}{H}\right)^2}\right),
\end{aligned} \tag{2}$$

where the subscripts "*S*", "*G*", "*W*" denote sky, ground, wall, respectively. For example, F_{GS} denotes the view factor for the ground to see the sky. H and R_d are the height of building and the width of the canyon, respectively.

Assuming that canyon orientations are uniformly distributed, *Masson* [2000] obtained analytical expressions for the direct solar fluxes for the wall ($S^{\Downarrow}_{W,dir}$) and the ground (including the vegetated part $S^{\Downarrow}_{P,dir}$ and the impervious part $S^{\Downarrow}_{IMP,dir}$):

$$S^{\Downarrow}_{W,dir}=S^{\Downarrow}_{dir}\left[\frac{R_d}{H}\left(\frac{1}{2}-\frac{\theta_o}{\pi}\right)+\frac{1}{\pi}\tan\left(\lambda\right)\left(1-\cos\theta_o\right)\right], \tag{3}$$

$$S^{\Downarrow}_{P,dir}=S^{\Downarrow}_{IMP,dir}=S^{\Downarrow}_{dir}\left[\frac{2\theta_o}{\pi}-\frac{2}{\pi}\frac{H}{R_d}\tan\left(\lambda\right)\left(1-\cos\theta_o\right)\right], \tag{4}$$

where θ_o is the critical canyon orientation for which the ground is no longer in the light or $\pi/2$ when the ground is always in the light, λ is the solar zenith angle. θ_o is calculated through:

$$\theta_o=\arcsin\left[\min\left(\frac{R_d}{H\tan\left(\lambda\right)},1\right)\right]. \tag{5}$$

The exchange of diffuse radiation within the urban canyon is parameterized based on the exact solution presented in *Harman et al*. [2004]. The downward and upward diffuse fluxes at each subcomponent are calculated as follows:

$$S^{\Downarrow}_{W,dif} = F_{WS}S^{\Downarrow}_{dif} + F_{WW}S^{\Uparrow}_{W,dif} + F_{WG}\left(f_P S^{\Uparrow}_{P,dif} + f_{IMP}S^{\Uparrow}_{IMP,dif}\right), \tag{6}$$

$$S^{\Downarrow}_{P,dif} = F_{GS}S^{\Downarrow}_{dif} + 2F_{GW}S^{\Uparrow}_{W,dif}, \tag{7}$$

$$S^{\Downarrow}_{IMP,dif} = F_{GS}S^{\Downarrow}_{dif} + 2F_{GW}S^{\Uparrow}_{W,dif}, \tag{8}$$

$$S^{\Uparrow}_{W,dif} = \alpha_{W,dif}S^{\Downarrow}_{W,dif} + \alpha_{W,dir}S^{\Downarrow}_{W,dir}, \tag{9}$$

$$S^{\Uparrow}_{P,dif} = \alpha_{P,dif}S^{\Downarrow}_{P,dif} + \alpha_{P,dir}S^{\Downarrow}_{P,dir}, \tag{10}$$

$$S^{\Uparrow}_{IMP,dif} = \alpha_{IMP,dif}S^{\Downarrow}_{g2,dif} + \alpha_{IMP,dir}S^{\Downarrow}_{IMP,dir}. \tag{11}$$

where $\alpha_{W,dir}$, $\alpha_{W,dif}$, $\alpha_{P,dir}$,$\alpha_{P,dif}$,$\alpha_{IMP,dir}$, and $\alpha_{IMP,dif}$ are the albedos for the wall, the pervious part of the ground, and the impervious part of the ground for direct and diffuse solar radiation. The above equations are solved analytically to obtain $S^{\Downarrow}_{W,dif}$, $S^{\Uparrow}_{W,dif}$, $S^{\Downarrow}_{P,dif}$, $S^{\Uparrow}_{P,dif}$, $S^{\Downarrow}_{IMP,dif}$, and $S^{\Uparrow}_{IMP,dif}$, which are the diffuse flux received by the wall, the diffuse flux leaving the wall, the diffuse flux received by the vegetated part of the ground, the diffuse flux leaving the vegetated part of the ground, the diffuse flux received by the impervious part of the ground, and the diffuse flux leaving the impervious part of the ground, respectively.

The net shortwave radiation received by the wall and the impervious part of the ground are:

$$S_W = \left(1-\alpha_{W,dir}\right)S^{\Downarrow}_{W,dir} + \left(1-\alpha_{W,dif}\right)S^{\Downarrow}_{W,dif}, \tag{12}$$

$$S_{IMP} = \left(1-\alpha_{IMP,dir}\right)S^{\Downarrow}_{IMP,dir} + \left(1-\alpha_{IMP,dif}\right)S^{\Downarrow}_{IMP,dif}, \tag{13}$$

The shortwave radiation received by the pervious part of the ground (i.e., $S^{\Downarrow}_{P,dir}$ and $S^{\Downarrow}_{P,dif}$) is further partitioned between vegetation and soil. The resulting solutions are as follows:

$$S_{veg} = S^{\Downarrow}_{P,dir}A_{veg,dir} + S^{\Downarrow}_{P,dif}A_{veg,dif}, \tag{14}$$

$$S_{soil} = S^{\Downarrow}_{P,dir}A_{soil,dir} + S^{\Downarrow}_{P,dif}A_{soil,dif}, \tag{15}$$

where the subscripts "*veg*" and "*soil*" indicate vegetation and soil, respectively. The coefficients $A_{veg,dir}$, $A_{veg,dif}$, $A_{soil,dir}$ and $A_{soil,dif}$ as well as albedos of the pervious part of the canyon $\alpha_{P,dir}$ and $\alpha_{P,dif}$ are calculated by solving the equations of radiation propagation through the canopy in two-stream approximation [*Milly et al*., 2014; *Shevliakova et al*., 2009]. As a result, they depend on the radiative properties of the vegetation and underlying soil, as well as other variables such as leaf area index (LAI), solar zenith angle (for direct radiation), and amount of snow on vegetation and ground.

For all man-made materials (i.e., roof, wall, and impervious ground), the albedos for direct and diffuse solar radiation are assumed to be identical (i.e., $\alpha_{R,dir}=\alpha_{R,dif}$, $\alpha_{W,dir}=\alpha_{W,dif}$, and $\alpha_{IMP,dir}=\alpha_{IMP,dif}$). In addition, unlike vegetation and soil that use different radiative properties for the visible and near-infrared ranges, man-made materials use the same radiative properties for both ranges in the current version of LM3-UCM.

2.3.2. Longwave Radiation

The net longwave radiation at the roof (I_R, W m^{-2}) is simply calculated as $I_R=\varepsilon_R I^{\Downarrow}-\varepsilon_R\sigma T_R^4$, where $I^{\Downarrow}$ is the downward longwave radiation from the atmosphere, ε_R is the emissivity of the roof surface, σ is the Stefan-Boltzmann constant, and T_R is the roof temperature (K). Within the urban canyon, the parameterization of longwave radiative exchange is similar to the parameterization of diffuse solar radiation. The upward and downward diffuse fluxes at each subcomponent ($I^{\Downarrow}_W$, $I^{\Uparrow}_W$, $I^{\Downarrow}_P$, $I^{\Uparrow}_P$,$I^{\Downarrow}_{IMP}$, $I^{\Uparrow}_{IMP}$) are first presented:

$$I^{\Downarrow}_W = F_{WS}I^{\Downarrow} + F_{WW}I^{\Uparrow}_W + F_{WG}\left(f_P I^{\Uparrow}_P + f_{IMP}I^{\Uparrow}_{IMP}\right), \tag{16}$$

$$I^{\Downarrow}_P = F_{GS}I^{\Downarrow} + 2F_{GW}I^{\Uparrow}_W, \tag{17}$$

$$I^{\Downarrow}_{IMP} = F_{GS} I^{\Downarrow} + 2F_{GW} I^{\Uparrow}_{W}, \tag{18}$$

$$I^{\Uparrow}_{W} = (1-\varepsilon_W) I^{\Downarrow}_{W} + \varepsilon_W \sigma T^4_W, \tag{19}$$

$$I^{\Uparrow}_{P} = I^{\Downarrow}_{P} A' + \varepsilon_{veg} \sigma T^4_{veg} B' + \varepsilon_{soil} \sigma T^4_{soil} C', \tag{20}$$

$$I^{\Uparrow}_{IMP} = (1-\varepsilon_{IMP}) I^{\Downarrow}_{IMP} + \varepsilon_{IMP} \sigma T^4_{IMP}, \tag{21}$$

where ε_W, ε_{veg}, ε_{soil} and ε_{IMP} are the emissivity of wall, vegetation, soil and the impervious ground, respectively. T_W, T_{veg}, T_{soil} and T_{IMP} are the temperatures (K) of wall, vegetation, soil and the impervious ground, respectively. The coefficients (A', B' and C') represent the interactions between vegetation and soil and hence depend on the reflectivity, emissivity and transitivity of vegetation and soil, whose calculations follow the LM3 model [*Milly et al*., 2014; *Shevliakova et al*., 2009].

The above equation system can be solved to obtain $I^{\Downarrow}_{W}$, $I^{\Uparrow}_{W}$, $I^{\Downarrow}_{P}$, $I^{\Uparrow}_{P}$,$I^{\Downarrow}_{IMP}$, $I^{\Uparrow}_{IMP}$. The net longwave radiation of the wall and the impervious ground is then calculated following:

$$I_W = I^{\Downarrow}_{W} - I^{\Uparrow}_{W} = \varepsilon_W I^{\Downarrow}_{W} - \varepsilon_W \sigma T^4_W, \tag{22}$$

$$I_{IMP} = I^{\Downarrow}_{IMP} - I^{\Uparrow}_{IMP} = \varepsilon_{IMP} I^{\Downarrow}_{IMP} - \varepsilon_{IMP} \sigma T^4_{IMP}, \tag{23}$$

The net longwave radiation of vegetation and soil is calculated through:

$$I_{veg} = I^{\Downarrow}_{P} A'_{veg} + \varepsilon_{veg} \sigma T^4_{veg} B'_{veg} + \varepsilon_{soil} \sigma T^4_{soil} C'_{veg}, \tag{24}$$

$$I_{soil} = I^{\Downarrow}_{P} A'_{soil} + \varepsilon_{veg} \sigma T^4_{veg} B'_{soil} + \varepsilon_{soil} \sigma T^4_{soil} C'_{soil}, \tag{25}$$

The coefficients A'_{veg}, B'_{veg}, C'_{veg}, A'_{soil}, B'_{soil} and C'_{soil} again represent interactions between vegetation and soil, whose calculations follow the LM3 model [*Milly et al*., 2014; *Shevliakova et al*., 2009].

2.3.3. Turbulent Exchanges

2.3.3.1. Turbulent Exchanges Between the Roof and the Atmosphere

The sensible heat flux (H_R, W m^{-2}) and evaporation rate (E_R, kg m^{-2} s^{-1}) from the roof are calculated from:

$$H_R = \rho c_p C_{h,R} (T_R - T_{atm}), \tag{26}$$

$$E_R = \rho C_{q,R} f_{l,R} \left(q^*(T_R) - q_{atm} \right), \tag{27}$$

where ρ is the air density (kg m^{-3}); c_p is the specific heat capacity of dry air at constant pressure (J kg^{-1} K^{-1}); T_R and $q^*(T_R)$ are the roof surface temperature (K) and the saturated specific humidity at the roof surface temperature (kg kg^{-1}), respectively; T_{atm} and q_{atm} are the temperature (K) and specific humidity (kg kg^{-1}) at the bottom level of the atmospheric model, respectively; $C_{h,R}$ and $C_{q,R}$ are the turbulent transfer coefficients (m s^{-1}) for sensible heat and water vapor, respectively, between the roof surface and the atmosphere; $f_{l,R}$ is the fraction of roof area occupied by liquid water.

The turbulent transfer coefficients (C_h and C_q) are calculated following Monin-Obukhov similarity theory and C_h and C_q are assumed to be identical. In this study, we used the same Monin-Obukhov similarity functions as in many other GFDL models [*GAMDT*, 2004]. However, parameterizations for the displacement height (d) and roughness lengths (i.e., momentum roughness length z_{om} and scalar roughness length z_{oh}), which are critical inputs for calculating C_h and C_q, are different from the existing parameterizations in LM3. For the roof, the displacement height is assumed to be zero and the momentum roughness length and the ratio of thermal to momentum roughness length are input parameters that need to be specified by users (see Table 2).

The fraction of roof area occupied by liquid water ($f_{l,R}$) is calculated following [*Bonan*, 1996]

$$f_{l,R} = \left(\frac{w_l}{w_{l,\max}} \right)^{p_l}, \tag{28}$$

where $p_l = 2/3$ is an empirical constant, w_l is the liquid water at the roof surface (kg m^{-2}), and $w_{l,max}$ is the maximum liquid water-holding capacity of the roof surface (kg m^{-2}).

2.3.3.2. Turbulent Exchanges Between the Urban Canyon and the Atmosphere

Turbulent exchanges of sensible heat (H_c, W m^{-2}), and water vapor (E_c, kg m^{-2} s^{-1}) between the urban canyon and the atmosphere are parameterized following:

$$H_c = \rho c_p C_h (T_c - T_{atm}), \tag{29}$$

$$E_c = \rho C_q (q_c - q_{atm}), \tag{30}$$

where T_c, and q_c are the canopy air temperature (K), and specific humidity (kg kg^{-1}) within the urban canyon, respectively; C_h, and C_q are the turbulent transfer coefficients (m s^{-1}) for sensible heat and water vapor, respectively, between the urban canyon and the atmosphere, which are again assumed to be identical and calculated following Monin-Obukhov similarity theory.

For the urban canyon, the displacement height (d) and roughness lengths (i.e., momentum roughness length z_{om} and scalar roughness length z_{oh}) are parameterized following [*MacDonald et al*., 1998]:

$$d = H\left(1 + A^{-\lambda_P}(\lambda_P - 1)\right), \tag{31}$$

$$z_{om} = H\left(1 - \frac{d}{H}\right)\exp\left[-\left(\frac{C_{dh}}{2\kappa^2}\left(1 - \frac{d}{H}\right)\lambda_F\right)^{-1/2}\right], \tag{32}$$

$$z_{oh} = \frac{1}{10} z_{om}, \tag{33}$$

where A (= 4) and C_{dh} (=1.2) are empirical constants and κ is the von-Karman constant [*Coceal and Belcher*, 2004]. λ_P and λ_F are the plan area density and the frontal area density, respectively, calculated as $\lambda_P = \frac{R_f}{R_f + R_d}$ and $\lambda_F = \frac{H}{R_f + R_d}$, where R_f and R_d are the roof width and the canyon width (i.e., road width), respectively.

2.3.3.3. Turbulent Exchanges Between Different Subcomponents and the Canopy Air in the Urban Canyon

Within the canyon, there are also turbulent exchanges between various subcomponents (i.e., vegetation, soil, impervious ground and wall) and the canopy air. The parameterizations of turbulent sensible and latent heat fluxes are similar to equations (29) and (30) except here temperature and specific humidity differences represent the differences between various subcomponents (i.e., vegetation, soil, impervious ground and wall) and the canopy air, respectively.

For example, turbulent fluxes between the impervious surface and the canopy air are calculated following:

$$H_{IMP} = \rho c_p C_{h,IMP} (T_{IMP} - T_c), \tag{34}$$

$$E_{IMP} = \rho C_{q,IMP} f_{l,IMP} (q^*(T_{IMP}) - q_c), \tag{35}$$

where $C_{h,IMP}$ and $C_{q,IMP}$ are the turbulent transfer coefficients (m s^{-1}) for sensible heat and water vapor, respectively, between the impervious surface and the canopy air within the urban canyon (assumed to be identical); T_{IMP} and $q^*(T_{IMP})$ are the impervious surface temperature (K) and the saturated specific humidity (kg kg^{-1}) at the impervious surface temperature, respectively; $f_{l,IMP}$ is the fraction of impervious surface area occupied by liquid water and is calculated in a similar way as equation (28). Similar to the roof surface, the displacement height of the impervious surface is assumed to be zero, and the momentum roughness length and the ratio of thermal to momentum roughness length are input parameters that need to be specified by users. However, the calculation of $C_{h,IMP}$ is not based on Monin-Obukhov similarity theory but follows its counterpart for the soil, as shall be discussed later.

Table 1. Urban Morphological Parameters for the Three Cities

	Marseille	Basel	UMBC
Canyon aspect ratio H/R_d	1.18	0.70	0.13
Roof fraction $R_f/(R_f+R_d)$	0.49	0.45	0.33
Vegetated ground fraction f_p	0.27	0.30	0.43
Building height H (m)	15.6	14.6	7.5
Roof substrate depth (m)	0.3	0.3	0.3
Wall substrate depth (m)	0.3	0.3	0.3
Road substrate depth (m)	0.5	0.5	0.5

[a]"Road" corresponds to the impervious ground in the LM3-UCM.

The sensible heat flux from the wall surface is calculated using the same turbulent transfer coefficient as for impervious surface, and the evaporation is assumed to be zero:

$$H_W = \rho c_p C_{h,IMP} (T_W - T_c), \tag{36}$$

$$E_W = 0, \tag{37}$$

The sensible heat flux (H_{soil}, W m^{-2}) and evaporation rate (E_{soil}, kg m^{-2} s^{-1}) from the soil are calculated as:

Table 2. Urban Surface Properties for the Three Cities[a]

	Marseille	Basel	UMBC
Roof emissivity	0.90	0.90	0.95
Wall emissivity	0.90	0.90	0.95
Road emissivity	0.94	0.94	0.95
Roof albedo	0.22	0.14	0.41
Wall albedo	0.20	0.14	0.25
Road albedo	0.08	0.08	0.28
Roof thermal conductivity (W m^{-1} K^{-1})	0.94	0.94	0.73
Wall thermal conductivity (W m^{-1} K^{-1})	0.94	0.94	1.30
Road thermal conductivity (W m^{-1} K^{-1})	0.5	0.5	1.51
Roof heat capacity (MJ m^{-3} K^{-1})	1.40	1.40	1.69
Wall heat capacity (MJ m^{-3} K^{-1})	1.40	1.40	1.20
Road heat capacity (MJ m^{-3} K^{-1})	1.80	1.80	1.73
Minimum building temperature (K)	301	297	297
Minimum building temperature (K)	301	297	297
Roof water holding depth (cm)	1	5	0.2
Road water holding depth (cm)	1	5	1
Roof momentum roughness length (m)	0.15	0.32	0.1
Road momentum roughness length (m)	0.05	0.05	0.01
Ratio of thermal to momentum roughness lengths for roof and road	1/1000	1/10	1/10

[a]"Road" corresponds to the impervious ground in the LM3-UCM.

$$H_{soil}=\rho c_p C_{h,soil}(T_{soil}-T_c), \quad (38)$$

$$E_{soil}=\rho C_{q,soil}(q_{soil}-q_c), \quad (39)$$

where $C_{h,soil}$ and $C_{q,soil}$ are the turbulent transfer coefficients (m s^{-1}) for sensible heat and water vapor, respectively, between soil and the canopy air within the urban canyon (assumed to be identical). The specific humidity at the soil surface (q_{soil}, kg kg^{-1}) is calculated based on the available water amount in the top layer of soil as in LM3 [*Milly et al.*, 2014].

The sensible heat flux (H_V, W m^{-2}) from the vegetation is calculated as:

$$H_{veg}=\rho c_p C_{h,veg}\left(T_{veg}-T_c\right), \quad (40)$$

The evapotranspiration from vegetation is given by $E_{veg}=E_t+E_l+E_s$, where E_t, E_l and E_s represent transpiration, evaporation of intercepted water and sublimation of intercepted snow, respectively (kg m^{-2} s^{-1}). They are calculated as:

$$E_t=\rho\frac{\left(1-f_{l,veg}-f_{s,veg}\right)}{1/C_{q,veg}+r_v}v(q^*(T_v)-q_c), \quad (41)$$

$$E_l=\rho f_{l,veg}C_{q,veg}(q^*(T_v)-q_c), \quad (42)$$

$$E_s=\rho f_{s,veg}C_{q,veg}(q^*(T_v)-q_c), \quad (43)$$

where $C_{h,veg}$ and $C_{q,veg}$ are the turbulent transfer coefficients (m s^{-1}) for sensible heat and water vapor, respectively, between vegetation and the canopy air within the urban canyon (assumed to be identical); $f_{l,veg}$ and $f_{s,veg}$ are the fractions of vegetation covered by liquid water and snow, respectively, which are calculated following *Bonan* [1996]; $q^*(T_{veg})$ is the saturated specific humidity at the vegetation temperature T_{veg}; r_v is the stomatal resistance. Carbon and vegetation dynamics are handled by a dynamic vegetation model as described by *Shevliakova et al.* [2009]. In addition, an urban vegetation management strategy is implemented into the dynamic vegetation model to enable studies of LULCC on urban vegetation. To mimic the human influence on the growth of vegetation in urban areas (e.g., mowing operations), we remove part of vegetation carbon and deposit it in the soil annually, leaving only 0.1 kg C/m^2 for future regrowth. Other strategies can be also implemented in the future.

The parameterizations of turbulent transfer coefficients for vegetation and soil follow the existing parameterizations in the LM3 model for the soil-vegetation-atmosphere continuum with some modifications to consider the existence of buildings. For vegetation, the turbulent transfer coefficient per unit leaf area is $\alpha\sqrt{u/d_l}$ [*Bonan*, 1996], where $\alpha=0.01$ m $s^{-1/2}$ is an empirical constant and d_l is the characteristic plant surface dimension in the streamwise direction (m); u is the wind speed profile (m s^{-1}) in the canyon. For an isothermal canopy, the total conductance is:

$$C_{h,veg}=\int_0^{h_{veg}}\alpha\sqrt{\frac{u(z)}{d_l}}LAD(z)dz=LAI\frac{2\alpha}{a}\sqrt{\frac{u(H)}{d_l}}\left(e^{-a\frac{H-h_{veg}}{2}{H}}-e^{-\frac{a}{2}}\right), \quad (44)$$

where h_{veg} is the vegetation height and is assumed to be smaller than the roof height H; LAD is the leaf area density (m^2/m^3), which is assumed to be uniform in the vertical direction and $LAI=\int_0^{\infty}LAD(z)dz$; a is an empirical parameter for the exponential wind speed (u) and turbulent diffusivity (K) profile in the urban canyon, that is, $u(z)=u(H)\exp\left(-a\frac{H-z}{H}\right)$ and $K(z)=K(H)\exp\left(-a\frac{H-z}{H}\right)$, which is calculated following *Coceal and*

Belcher [2004]. $u(H)$ is the wind speed at the top of the urban canyon and is computed from $u(H)=\frac{u_*}{\kappa}log\left(\frac{H-d}{z_{om}}\right)$, where κ is again the von-Karman constant; u_* is the friction velocity (m s^{-1}); d is the displacement height of the urban canyon (m); z_{om} is the momentum roughness length of the urban canyon (m). $K(H)$ is the turbulent diffusivity at the top of the urban canyon and is computed from $K(H)=\kappa u_*(H-d)$.

For the soil, the inverse of turbulent transfer coefficient (i.e., the resistance) is computed by integrating the inverse of turbulent diffusivity from $z_{oh,soil}$, which is the scalar roughness length of soil, to $z_1=z_{om}+d$, and the resulting turbulent transfer coefficient is

$$C_{h,soil}=\frac{\kappa u_*(H-d)a}{H}\frac{1}{e^{a\left(1-z_{oh,soil}/H\right)}-e^{a(1-z_1/H)}}. \tag{45}$$

2.3.4. Ground Heat Fluxes

In this study, we consider the heat transport in impervious materials through diffusion. When calculating ground heat fluxes, we adopt the convention that z increases downward, and the flux is also positive downward. The one-dimensional diffusion equation for heat is:

$$c\frac{\partial T}{\partial t}=-\frac{\partial}{\partial z}\left(-\lambda\frac{\partial T}{\partial z}\right), \tag{46}$$

where c is the heat capacity of the substrate (J m^{-3} K^{-1}), λ is the thermal conductivity (W m^{-1} K^{-1}), and T is the substrate temperature (K). The above equation is discretized and solved numerically at five uniform levels for the roof, the wall and the impervious ground, whose thicknesses are specified by the users. The equations for heat and flux conductance in soil and snow (if present) follow *Milly et al*. [2014]. For the impervious ground, the bottom boundary conditions are heat fluxes from/into the underlying soil.

For the roof and walls, the bottom boundary conditions can be specified as either "no-flux" or "constant temperature." The "constant temperature" boundary conditions represent the scenario where the building interior temperature is set to be constant or within a range specified by the maximum and minimum building interior temperatures. Using the option of "constant temperature" as boundary conditions implies that there may be a source or sink of anthropogenic heat in the urban system [*Oleson*, 2012; *Oleson et al*., 2011]. This anthropogenic heat flux can be significant under certain climatic conditions, as will be shown in Part II of our study. In our model, the temperatures of the most inner layers of roof and wall are area-averaged to yield the building temperature, following the method of CLMU [*Oleson et al*., 2008].

2.3.5. Hydrology

2.3.5.1. Snow

Snow processes are parameterized as in LM3 [*Milly et al*., 2014] with one additional modification: in the UCM snow is allowed on the roof and the pervious ground, while the snow on the impervious ground goes to runoff immediately. When snow is present on the roof or the pervious ground, the heat transport in snow is calculated with heat flux from the roof or the pervious ground as bottom boundary conditions. Snow also affects albedo and roughness lengths, which are accounted for using the same parameterizations in LM3 [*Milly et al*., 2014].

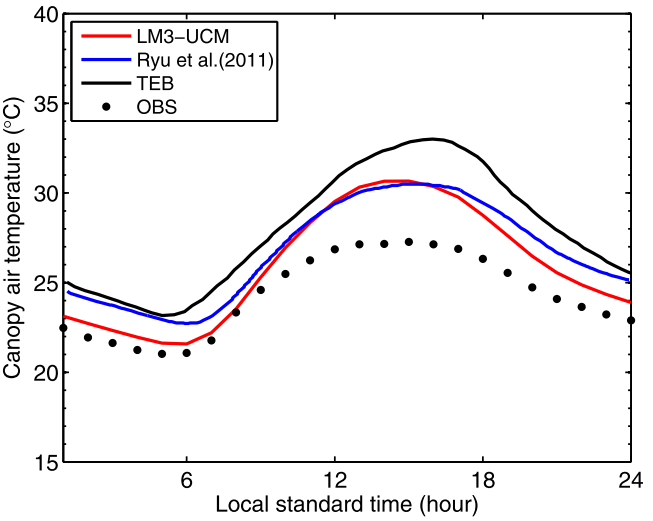

Figure 2. Averaged diurnal cycles of canyon air temperature in the urban canyon observed and simulated by UCMs in Marseille, France from 18 June to 11 July 2001. The observations are averaged over five in-canyon stations.

2.3.5.2. Runoff

Runoff generated from soil and snow follows existing parameterizations and calculations in LM3 [*Milly et al*., 2014]. The wall surface does not generate runoff. For the roof and the impervious ground, the runoff is calculated following:

$$\frac{dw_l}{dt}=P_l-E_l-R_l, \tag{47}$$

where w_l is the liquid water intercepted by the roof and impervious

surfaces (kg m^{-2}) and is capped by $w_{l,\max}$. P, E and R are precipitation, evaporation and runoff (kg m^{-2} s^{-1}), respectively. Runoff only occurs when $w_l > w_{l,\max}$. Note $w_{l,\max}$ can be different for the roof and the impervious ground depending on the materials and are required model parameters. Due to phase change, liquid water on the roof and the impervious ground might become frozen water (w_s). The frozen water is removed to runoff when $w_s > w_{s,\max}$. Similarly, $w_{s,\max}$ can be different for the roof and the impervious ground.

2.4. Overview of Solution Procedure

The conservation equations for canopy air specific humidity and sensible heat are:

$$m_c \frac{dq_c}{dt} = f_P\left(E_{veg} + E_{soil}\right) + f_{IMP}E_{IMP} - E_c, \tag{48}$$

$$\begin{aligned} m_c \frac{d}{dt}\left[(1-q_c)c_pT_c + q_c c_v T_c\right] = \frac{2H}{R_d}H_w + f_P\left(H_{veg} + H_{soil}\right) + f_{IMP}H_{IMP} - H_c \\ + c_v\left(f_P T_{veg}E_{veg} + f_P T_{soil}E_{soil} + f_{IMP}T_{IMP}E_{IMP} - T_c E_c\right), \end{aligned} \tag{49}$$

where m_c is the mass of the canopy air per unit area (kg m^{-2}); c_v is the specific heat capacity of water vapor at constant pressure (J kg^{-1} K^{-1}).

For each time step, these conservation equations together with the energy balance equations for the roof surface, the wall surface, the impervious ground surface, the soil surface and the vegetation, as well as the water balance equations for vegetation are solved simultaneously and implicitly. Next, potential phase changes at all surfaces are identified and dealt with, and runoff is computed. At the end, coupling with snowpack and the whole substrate column in terms of heat exchange is performed.

2.5. Dynamic Transition of Urban Tiles

As mentioned in section 2.1, a unique requirement associated with developing an urban parameterization for GCMs or ESMs is that the area of urban tiles must be dynamic in order to represent transitions from rural land to urban land and sometimes vice versa in multidecadal or multicentury simulations. In our model, a fraction of vegetation tile area (i.e., cropland, pasture, natural, or secondary vegetation) can become urban area. Occasionally part of the urban tile can undergo transition to one of vegetation tiles (in rare cases of urban abandonment). The annual rates of these urban transitions, as well as transition rates among the vegetation tiles are prescribed following historical reconstruction and future scenarios [*Hurtt et al*., 2011].

During these transitions, energy, water and carbon are conserved. When a part of nonurban tile is converted to an urban tile, the vegetation carbon and the water intercepted by vegetation are moved to the soil. The initial temperatures of the impervious facets (i.e., roof, wall, impervious ground) are assumed to be identical to the soil surface temperature of the original nonurban tile. The difference between the original tile energy and the energy of new urban tile (i.e., due to initialization of impervious surfaces) is made up by adjusting the soil temperature using the depth of soil layers as weights. On the other hand, if an urban tile turns into a nonurban, the water held by the roof and the impervious ground is moved to the soil. Again, the difference in energy due to removal of urban assets is made up by adjusting the temperature of the soil.

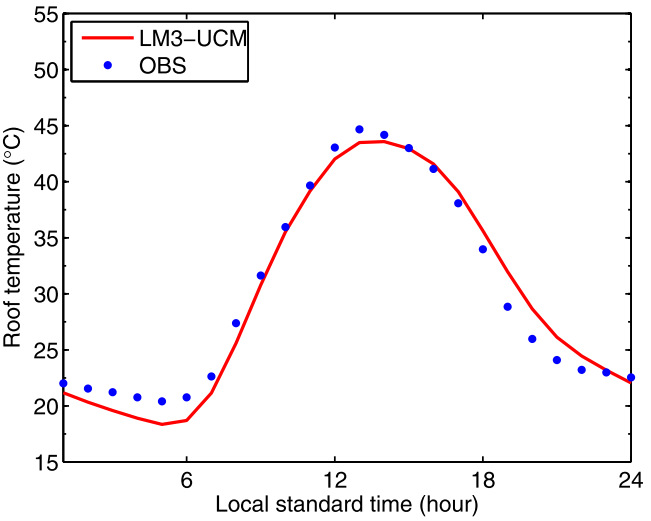

Figure 3. Averaged diurnal cycles of roof surface temperature observed and simulated by LM3-UCM in Marseille, France from 28 June to 11 July 2001. The observations are averaged over five tile roofs.

If the grid cell already has existing urban tiles, then a new urban tile generated by transitions is merged with an existing urban tile of the same type. In the current version of our model, only

one urban type is allowed per grid cell. This is because transition rates only provide one type of urban [*Hurtt et al*., 2011]. That is, there is no information about whether land use transitions convert nonurban area to low density urban or high density urban, or a combination of both. As a result, currently the new urban tile will be always merged with the existing urban tile.

The properties of urban tiles are either prescribed as global constants, or come from a global data set. For example, in Part II of our study, a global data set of urban properties developed by *Jackson et al*. [2010] is used for simulations over the Continental United States. In the future, multiple types of urban surface per grid cell (e.g., high density urban and low density urban) can be introduced to better represent subgrid urban surface heterogeneity. The global data set of urban surface properties developed by *Jackson et al*. [2010] actually includes four types of urban (i.e., tall building district, high density, medium density, and low density urban) to support this capability. However, the partition of land use transitions among different types of urban area, as well as transitions among different type of urban areas, are not well constrained. These topics are left for future research.

3. Model Evaluation

In this section, the LM3-UCM described in section 2 is used to conduct simulations in three cities: Marseille in France, Basel in Switzerland and Baltimore in the United States. These three sites are chosen because they have been studied in previous work and the observational data are available to us. The model is forced by observational data, including precipitation, air pressure, incoming shortwave radiation, incoming longwave radiation, wind speed, air temperature and specific humidity. The simulated results in terms of canopy air and surface temperatures, outgoing shortwave/longwave radiation and turbulent fluxes are then compared to observations and/or simulated results from other UCMs.

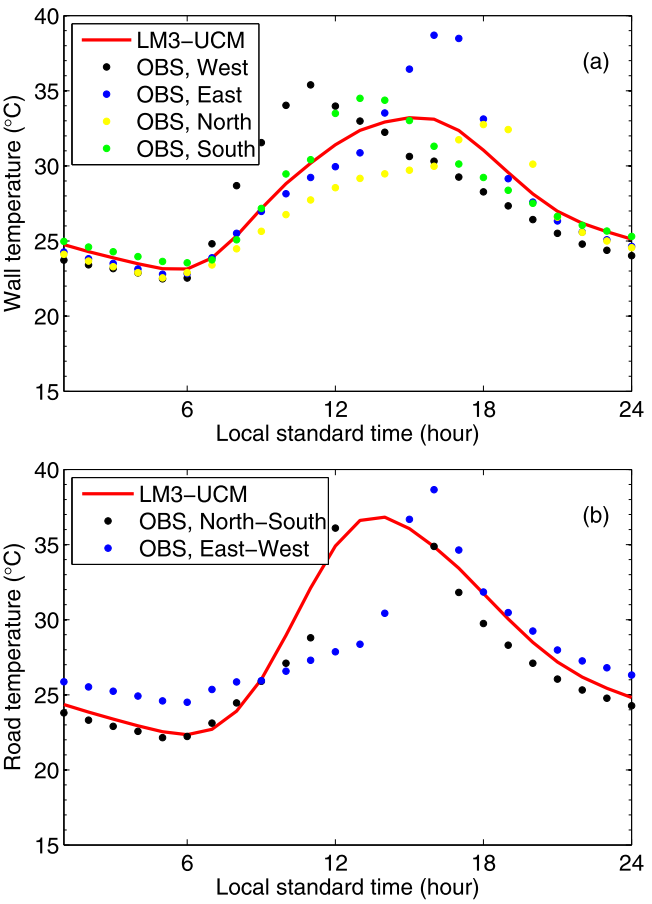

Figure 4. Averaged diurnal cycles of (a) wall surface temperature and (b) impervious ground surface temperature observed and simulated by LM3-UCM in Marseille, France from 28 June to 11 July 2001. The observations of wall surface temperature are taken from four walls that face different directions, while the observations of impervious ground surface temperature are taken from two roads along different directions.

For short-period simulations, previous studies have reported that model initialization, especially soil moisture initialization, has a substantial impact on urban models' performance [*Best and Grimmond*, 2014]. To evaluate the importance of model initialization for the Marseille and Basel sites, two approaches for model initialization are tested. In the first method, LM3-UCM is started with roof, wall, and impervious ground temperatures initialized at 15°C and the volumetric soil moisture of the pervious ground initialized at 0.5 m^3 m^{-3} (i.e., the soil is wet) at the beginning of the numerical experiments. The initial LAI values are assumed to be about 0.4 and 0.7 for the Marseille and Basel sites, respectively, which grow to about 0.7 and 1.0 at the end of the numerical experiments. In the second method, the same initialization as in the first method was followed by a 3

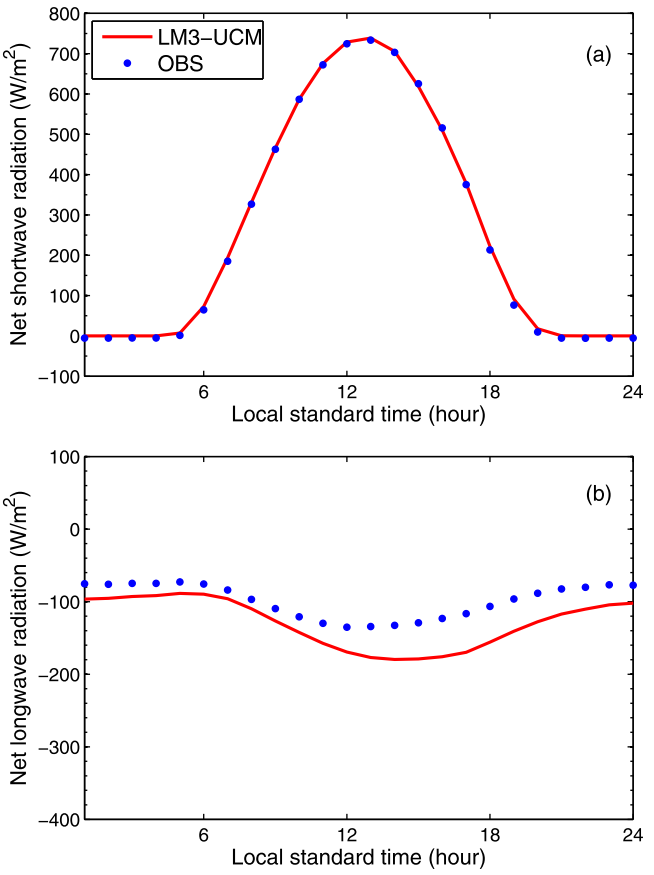

Figure 5. Averaged diurnal cycles of (a) net shortwave radiation and (b) net longwave radiation observed and simulated by the LM3-UCM in Marseille, France from 18 June to 11 July 2001.

year spin-up driven by the atmospheric forcing from *Sheffield et al.* [2006]. The final state of this spin-up was then used as initial conditions for the numerical experiments. The results at the Basel site are very similar for these two initialization methods and are also not sensitive to the initial soil moisture in the first method since it rains at the very beginning of the simulation period, which reduces the influence of initial soil moisture. The results at Basel are also not very sensitive to the initial LAI: doubling the initial LAI only increases the mean latent heat flux by 2.5 W m^{-2}. Nonetheless, the evaporation at the Marseille site is strongly affected by the initial soil moisture, which is partly related to the fact that there is no rain at Marseille during the simulation period. The 3 year spin-up period at the Marseille site reduces the initial soil moisture to almost the wilting point and thus reduces the evapotranspiration in the simulation period to nearly zero. There are two probable causes for the difference between two initialization approaches at Marseille: first, the soil properties used in the model may not reflect the real situation given that the soil data have a fairly low resolution; second, irrigation for urban vegetation is not considered. Without any further information about the initial soil moisture, results from the first method are presented here but it is noted here that the simulated evaporation at Marseille is sensitive to the initialization of soil moisture. The influence of initial LAI at Marseille is less important since doubling the initial LAI only increases the mean latent heat flux by 3.6 W m^{-2}. At the Baltimore site, the model initial state is taken from *Ramamurthy et al.* [2014] with the initial LAI set to be about 1, which was also used by *Ramamurthy et al.* [2014] (Dr. P. Ramamurthy, personal communication, 2015; since *Ramamurthy et al.* [2014] did not report LAI in their paper).

3.1. Marseille, France

Measurements of atmospheric forcing from the urban boundary-layer field campaign in Marseille, France from 18 June to 11 July 2011 [*Grimmond et al.*, 2004; *Hamdi and Schayes*, 2007; *Lemonsu et al.*, 2004; *Mestayer et al.*, 2005] are used to drive the LM3-UCM. The measurement site was located at the down-town core of Marseille and over a complex geographic setting [*Lemonsu et al.*, 2004]. The data were collected on a pneumatic tower over the roof of a tall building (base of the tower was 20.7 m above the ground level), including eddy covariance measurements that allow turbulent fluxes to be calculated [*Lemonsu et al.*, 2004]. The urban morphological parameters (Table 1) and surface properties used by LM3-UCM (Table 2) are principally adopted from the studies by *Lemonsu et al.* [2004], *Hamdi and Schayes* [2007], and *Ryu et al.* [2011], which were conducted over the same site. Note that the model is capable of representing different materials within a wall or a roof since it solves the thermal diffusion equation by discretizing the wall or the roof into five layers that can have different properties and thickness. However, for the cases studied here, the same thermal properties are used for all layers due to the lack of data for each layer. The urban morphological parameters (Table 1) are slightly different from those used by *Lemonsu et al.* [2004],

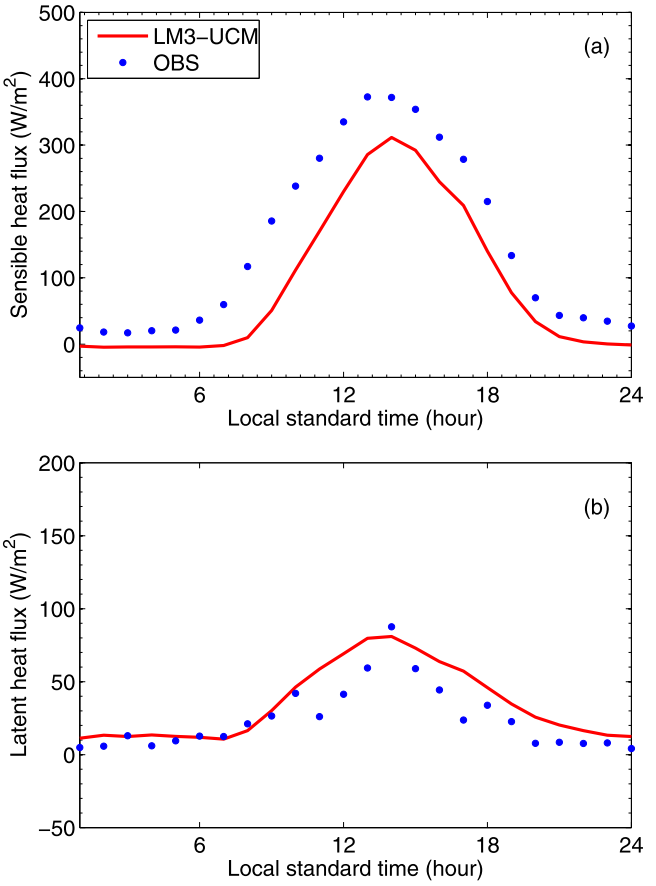

Figure 6. Averaged diurnal cycles of (a) sensible heat flux and (b) latent heat flux observed and simulated by LM3-UCM in Marseille, France from 18 June to 11 July 2001.

Hamdi and Schayes [2007], and *Ryu et al.* [2011], to account for the differences in model structures: the Town Energy Balance (TEB) model used by *Lemonsu et al.* [2004] and *Hamdi and Schayes* [2007], and the single-layer UCM developed by *Ryu et al.* [2011] assume vegetation is outside of the urban canyon while our model includes vegetation as an integrated part of the canyon. As a result, changes are made to some morphological parameters in our simulations to accommodate this change (see Table 1). In addition, the internal building temperature is set to be 28°C based on Figure 6 in *Lemonsu et al.* [2004], and the ratio of thermal to momentum roughness length is also chosen based on the discussions in *Lemonsu et al.* [2004].

Figure 2 shows the canyon air temperatures simulated by the LM3-UCM, the TEB model [*Lemonsu et al.*, 2004] and the single-layer UCM proposed by *Ryu et al.* [2011], and observations averaged over five in-canyon stations. It is clear that all UCMs overestimate the daytime canyon air temperature. The initial version of TEB [*Lemonsu et al.*, 2004] and the single-layer UCM proposed by *Ryu et al.* [2011] also overestimates the nighttime canyon air temperature, while the LM3-UCM captures the nighttime canyon air temperature better than the other two models. As discussed in *Lemonsu et al.* [2004], the overestimation of the canyon air temperature in the daytime is due to insufficient ventilation of the heat from the urban canyon to the atmosphere. When a new formulation that allows heat released from the walls and ground to be freely vented from the urban canyon to the atmosphere was used in TEB, the daytime results were significantly improved [see *Lemonsu et al.*, 2004, Figure 4]. Similar sensitivity tests are conducted with our LM3-UCM and similar improvements are observed (not shown), which suggests that parameterizing the thermal roughness length in urban areas remains a challenge and traditional parameterizations for bare soil and vegetation canopies might not work properly over complex heterogeneous urban terrain. This is consistent with previous studies [see e.g., *Li and Bou-Zeid*, 2014].

Figure 3 shows the comparison between the LM3-UCM simulated roof surface temperature and observations averaged from 28 June to 11 July 2011. It is evident that the model correctly reproduces the observed diurnal cycle of roof surface temperatures averaged over five roofs. Figure 4 shows the comparison between simulated wall and impervious ground surface temperature and observations. The model results fall into the range of the observations, implying that the model is able to capture the general variations of wall and impervious ground surface temperatures. Note that the LM3-UCM was constructed to simulate spatially averaged temperatures, assuming the urban canyon

Table 3. Mean Bias Errors (MBE) and Root-Mean-Square Errors (RMSE) of Simulated Sensible and Latent Heat Fluxes (units: W m^{-2})

		Marseille	Basel	UMBC
H	MBE	−60.4	−11.6	−11.9
	RMSE	69.5	40.0	34.9
LE	MBE	9.8	1.5	0.9
	RMSE	51.5	26.0	27.9

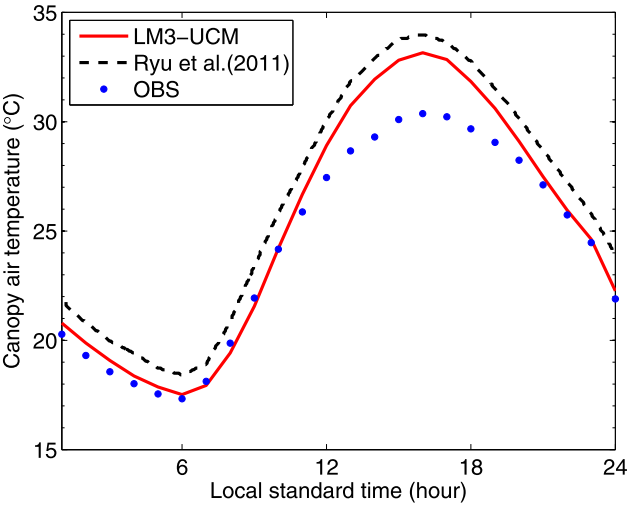

Figure 7. Averaged diurnal cycles of canopy air temperature in the urban canyon observed and simulated by two UCMs in Basel, Switzerland over 10 clear days: 164, 165, 168, 169, 170, 174, 177, 181, 186 and 189 (day of year).

orientations follow a uniform distribution, while the observations are taken at specific canyon orientations, as noted in the Figure 4. This may explain the wide range of observations, and part of the differences with model results.

Figure 5 shows the comparison between simulated and observed net shortwave (Figure 5a) and longwave (Figure 5b) radiation averaged over the study period. The averaged diurnal cycle of net shortwave radiation is well captured by the model, which implies that the albedo values used by the model are more or less correct. However, the averaged diurnal cycle of net longwave radiation is more negative in the simulation, which implies that the outgoing longwave radiation is overestimated by the model and is thus consistent with the overestimation of canopy air temperature in the canyon. The overestimation of outgoing longwave radiation at Marseille has been also observed in previous studies using other UCMs [*Lemonsu et al*., 2004; *Ryu et al*., 2011].

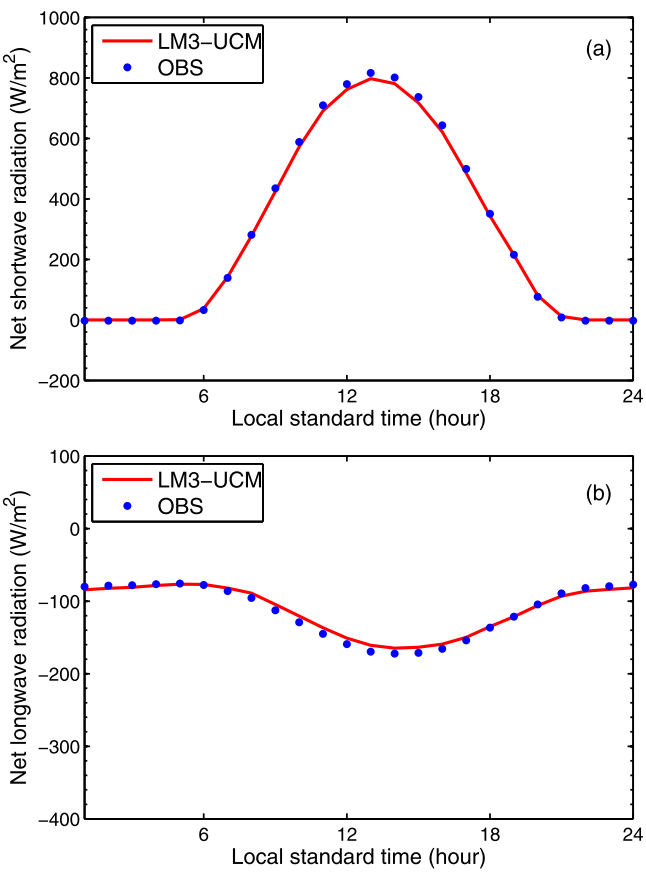

Figure 8. Averaged diurnal cycles of (a) net shortwave radiation and (b) net longwave radiation observed and simulated by the LM3-UCM in Basel, Switzerland over 10 clear days.

It is further shown in Figure 6 that the model reasonably captures the sensible heat flux (Figure 6a) and latent heat flux (Figure 6b) averaged over the observational period. It appears that the model underestimates the sensible heat flux at both daytime and nighttime. Part of these discrepancies might be due to neglecting some aspects of anthropogenic heat fluxes (e.g., from transportation) in our simulation. Note the internal building temperature is prescribed to be 28°C in our simulation thereby creating anthropogenic heat fluxes. *Lemonsu et al*. [2004] used the approach of *Grimmond* [1992] to estimate anthropogenic heat fluxes in Marseille, France and showed that anthropogenic heat fluxes were less than 15 W m^{-2} in the daytime and 2 W m^{-2} at nighttime. However, it is noted that there are generally large uncertainties associated with estimation of anthropogenic heat fluxes [*Nie et al*., 2014; *Sailor*, 2011]. The sudden drop of latent heat flux in observations around 11AM is not captured by our model, which may be also due to some measurement issues. The mean bias errors (MBEs, defined as the

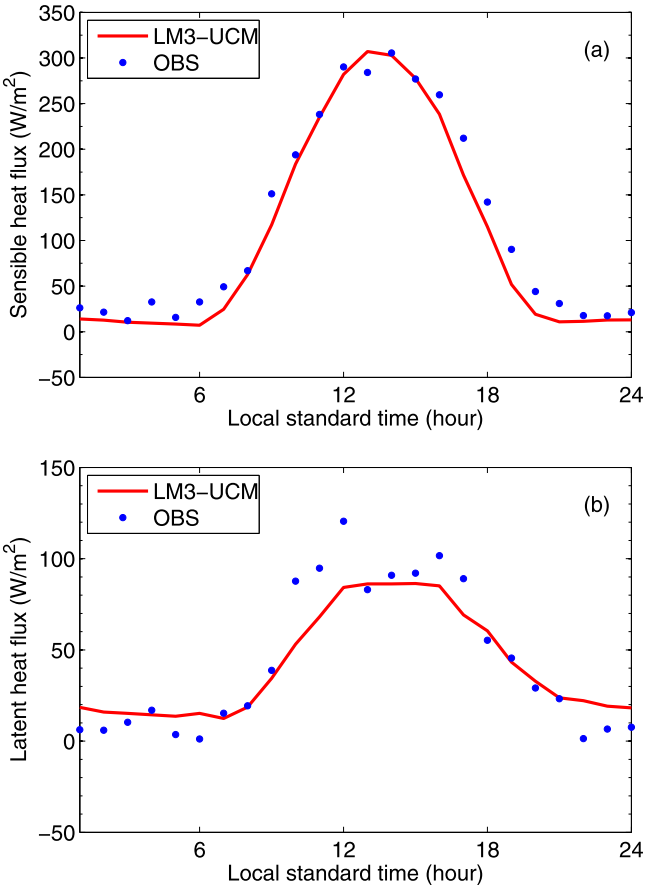

Figure 9. Averaged diurnal cycles of (a) sensible heat flux and (b) latent heat flux observed and simulated by the LM3-UCM in Basel, Switzerland over 10 clear days.

differences between simulations and observations) and root-mean-square errors (RMSEs) for sensible and latent heat fluxes are presented in Table 3. Our results for sensible and latent heat fluxes are generally comparable to two previous modeling studies [*Lemonsu et al.*, 2004; *Ryu et al.*, 2011] but our model overestimates the latent heat flux on average (i.e., the MBE for latent heat flux is positive) while the other two models generally underestimate the latent heat flux. This might be related to how the model is initialized since the initial soil moisture has a strong impact on the simulated latent heat flux at this site. When the initial soil moisture is reduced from 0.5 m^3 m^{-3} to 0.3 m^3 m^{-3}, the MBE for latent heat flux becomes -7.0 W m^{-2} (i.e., LM3-UCM now underestimates the latent heat flux) and the RMSE becomes 51.8 W m^{-2}.

3.2. Basel, Switzerland

In this section, the atmospheric forcing and other observations taken from the BUBBLE (Basel UrBan Boundary Layer Experiment) field campaign during 2001–2002 [*Christen and Vogt*, 2004; *Rotach et al.*, 2005] are used to drive and validate LM3-UCM. A micrometeorological tower was operated over a heavily built-up part of the Basel city (Basel-Sperrstrasse), which includes mainly residential 3–4 story buildings in blocks, flat commercial and light industrial buildings in the backyards (https://mcr.unibas.ch/Projects/BUBBLE/textpages/ob_frameset.en.htm). In our study, measurements over the intensive observation period (IOP) from 10 June to 10 July 2002 are used (http://ibis.geog.ubc.ca/~achristn/research/BUBBLE/data.html), which have been used in previous studies for validating TEB [*Hamdi and Schayes*, 2007] and the single-layer UCM developed by *Ryu et al.* [2011]. Morphological parameters and surface properties are taken from *Hamdi and Schayes* [2007] with similar modifications to accommodate the fact that vegetation is inside the urban canyon in LM3-UCM (see Tables 1 and 2). In addition, we also calculated the momentum roughness length of the roof using the standard deviation of building heights (σ_H=6.9 m, see https://mcr.unibas.ch/Projects/BUBBLE/textpages/ob_frameset.en.htm), with equation (32) and $\lambda_F = \frac{\sigma_H}{R_f + R_d}$.

Figure 7 shows the validation of simulated canopy air temperatures from the LM3-UCM and the UCM proposed by *Ryu et al.* [2011] averaged over 10 clear days. It is clear that the LM3-UCM captures the general diurnal variation of the canopy air temperature but shows some overestimation during the peak hours in the daytime. However, compared to the simulated results from *Ryu et al.* [2011], LM3-UCM yields a smaller bias. *Hamdi and Schayes* [2007] only showed the comparison for a 2 day period (17 and 18 June); the results of LM3-UCM for the same 2 day period are comparable to their results (not shown).

Figure 8 shows the comparison of net shortwave (Figure 8a) and longwave radiation (Figure 8b) simulated by LM3-UCM and measured at the meteorological tower averaged over 10 clear days. It is clear that the net shortwave and longwave radiation are well captured by LM3-UCM. Figure 9 shows the comparison in terms of sensible heat flux (Figure 9a) and latent heat flux (Figure 9b). LM3-UCM again agrees well with the measured diurnal cycles of sensible and latent heat fluxes. Similar to Figure 6b, the sudden drop of latent heat

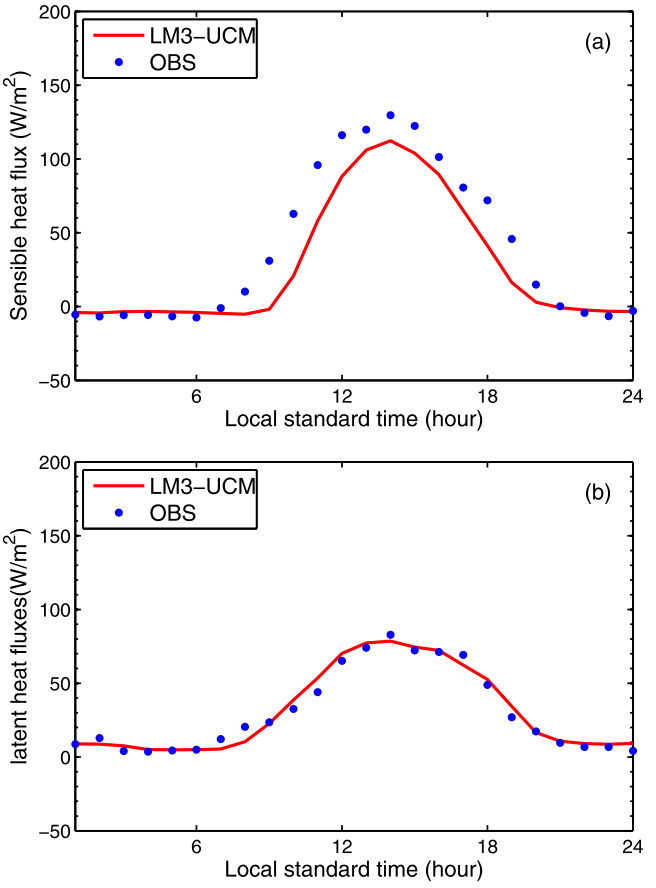

Figure 10. Averaged diurnal cycles of (a) sensible heat flux and (b) latent heat flux observed and simulated by the LM3-UCM at UMBC over 21 clear days.

flux in observations around 12 pm is not captured by our model, which again may be simply due to measurement issues. The MBEs and RMSEs for sensible and latent heat fluxes are presented in Table 3. Overall, our results are slightly better than those in *Ryu et al.* [2011]. As compared to the results in *Hamdi and Schayes* [2007] who compared simulations to observations over 5 clear days, our RMSE for sensible heat flux is larger while the RMSE for latent heat flux is lower.

3.3. Baltimore, USA

A micrometeorological tower was set up over the University of Maryland at Baltimore County (UMBC), which is a relatively low-density urban area, compared to the city of Basel. The measurements from the tower during July 2009 have been used to evaluate the Princeton Urban Canopy Model (PUCM) in two recent studies [*Ramamurthy and Bou-Zeid*, 2014; *Ramamurthy et al.*, 2014]. In this study, we follow the same methodology used in these two studies. However, since the LM3-UCM cannot simulate multiple roof (e.g., white roof and black roof) and impervious ground facets (i.e., asphalt and concrete), we aggregate the fractions and properties of these roof and impervious ground facets into a single roof facet and a single impervious ground facet. The aggregated fractions and properties are then used for LM3-UCM (see Tables 1 and 2). Also, in contrast to *Ramamurthy et al.* [2014], we do not separate the footprint of the UMBC flux tower into different sectors and account for different land cover characteristics. Instead, we use the averaged land cover fractions in the footprint.

Figure 10 shows the comparison between simulated and measured sensible heat flux (Figure 10a) and latent heat flux (Figure 10b). The results are averaged over 21 clear days in the month of July 2009 when the quality of flux data is good, which is in contrast to *Ramamurthy et al.* [2014] who examined the averaged diurnal cycles over the whole month. As can be seen, the LM3-UCM reasonably captures the diurnal variations of sensible and latent heat fluxes. However, the sensible heat fluxes are slightly underestimated by our UCM, which might be again related to neglecting anthropogenic heat fluxes in the model. The MBEs and RMSEs for sensible and latent heat fluxes are generally comparable to those in *Ramamurthy and Bou-Zeid* [2014], with a slightly larger RMSE for sensible heat flux in our study.

4. Conclusions

This is the first part of a series exploring historical and future urban climate within GFDL's Earth System Modeling framework, which is motivated by the fact that many current GCMs and ESMs do not have any urban representations. In this part, a new urban canopy model (LM3-UCM) is described, evaluated and incorporated into land component of the GFDL ESMs. The UCM is based on the urban canyon concept and has two unique features: first, it is coupled to a dynamic vegetation model so that it allows for the study of the effects of human activities on urban vegetation through urban vegetation management strategy; second, it can simulate the "urban sprawl" effect by allowing transitions between urban and vegetation tiles.

The second feature is a key for investigating the long-term impacts of urbanization on the climate, which will be presented in the second part of our study.

Using offline simulations forced by measured atmospheric fields, the LM3-UCM is validated at three cities: Marseille in France, Basel in Switzerland, and Baltimore in the United States. Results indicate that the model is able to reproduce diurnal cycles of canyon air temperature, surface temperatures, radiative fluxes and turbulent fluxes reasonably well. Compared to other UCMs, our model has a comparable performance. However, the results also show that some elements of the model, such as the parameterization of momentum and scalar roughness lengths, despite their importance, are poorly understood. In addition, model initialization plays an important role in altering the simulated surface energy balance at some sites (e.g., Marseille), since these simulations (like in many other model validation studies) are essentially short runs.

Future investigations are strongly needed to understand key processes such as turbulent transport of heat and water vapor in urban areas and improve their parameterizations. Better characterization of urban soil properties and measurements of urban soil moisture are also strongly needed for improving our model and validating the model results. In addition, model evaluation was only conducted over three midlatitude cities and over summer seasons, which is a typical limitation of this type of studies. Future work involves evaluating urban simulations in cities of different morphologies and background climates using long-term observational data sets. Last but not least, similar to many other UCMs, LM3-UCM needs a large number of inputs that can be highly variable in space and time (see Tables 1 and 2). When implementing it into global ESMs, a global data set that includes all these parameters needed by LM3-UCM is required. As will be shown in Part II, a global data set of urban properties developed by *Jackson et al*. [2010] is used for urban simulations over the Continental United States. In addition, on-going efforts and initiatives such as The World Urban Database and Access Portal Tools (WUDAPT, http://www.wudapt.org) to collect urban data will further enhance our capability of capturing and predicting urban climate.

Acknowledgments

Support from the NOAA (U.S. Department of Commerce) grant NA08OAR4320752 and the Carbon Mitigation Initiative at Princeton University, sponsored by BP, is acknowledged. The statements, findings, and conclusions are those of the authors and do not necessarily reflect the views of the NOAA, the U.S. Department of Commerce or BP. We thank Prathap Ramamurthy at The City College of New York for helpful discussions. We thank Young-Hee Ryu at National Center for Atmospheric Research for constructive suggestions and for her kind help with obtaining and understanding the observational data. We also would like to thank the teams that collected the observational data in Marseille and Basel. The core project of BUBBLE was funded by the Swiss Ministry of Education and Science (grant C00.0068) and the University of Basel, the Swiss Federal Institute of Technology (ETH) Zürich, the Technical University of Dresden, and the Bulgarian National Institute of Meteorology and Hydrology all contributed to the data set. We thank Professor Claire Welty, Julia Miller and Joshua Cole from UMBC/CUERE for providing the Baltimore data set. We thank the two anonymous reviewers whose comments led to significant improvement of our paper. The code and simulation results can be obtained from the corresponding author.

References

Arnfield, A. J. (2003), Two decades of urban climate research: A review of turbulence, exchanges of energy and water, and the urban heat island, *Int. J. Climatol.*, *23*(1), 1–26, doi:10.1002/joc.859.

Balaji, V., J. Anderson, I. Held, M. Winton, J. Durachta, S. Malyshev, and R. Stouffer (2006), The FMS Exchange Grid: A mechanism for data exchange between Earth System components on independent grids, in *Proceedings of the 2005 International Conference on Parallel Computational Fluid Dynamics*, Elsevier, College Park, Md.

Best, M. J., and C. S. B. Grimmond (2014), Importance of initial state and atmospheric conditions for urban land surface models' performance, *Urban Clim.*, *10*, Part 2, 387–406, doi:10.1016/j.uclim.2013.10.006.

Best, M. J., C. S. B. Grimmond, and M. G. Villani (2006), Evaluation of the urban tile in MOSES using surface energy balance observations, *Boundary Layer Meteorol.*, *118*(3), 503–525.

Bonan, G. B. (1996), A land surface model (LSM Version 1.0) for ecological, hydrological, and atmospheric studies: Technical description and user's guide, *NCAR Tech. Note NCAR/TN-417+STR*, doi:10.5065/D6DF6P5X.

Bou-Zeid, E., J. Overney, B. D. Rogers, and M. B. Parlange (2009), The effects of building representation and clustering in large-eddy simulations of flows in urban canopies, *Boundary Layer Meteorol.*, *132*(3), 415–436, doi:10.1007/S10546-009-9410-6.

Christen, A., and R. Vogt (2004), Energy and radiation balance of a central European city, *Int. J. Climatol.*, *24*(11), 1395–1421, doi:10.1002/joc.1074.

Coceal, O., and S. E. Belcher (2004), A canopy model of mean winds through urban areas, *Q. J. R. Meteorol. Soc.*, *130*(599), 1349–1372, doi:10.1256/qj.03.40.

Demuzere, M., K. Oleson, A. M. Coutts, G. Pigeon, and N. P. M. van Lipzig (2013), Simulating the surface energy balance over two contrasting urban environments using the Community Land Model Urban, *Int. J. Climatol.*, *33*(15), 3182–3205, doi:10.1002/joc.3656.

Findell, K. L., E. Shevliakova, P. C. D. Milly, and R. J. Stouffer (2007), Modeled impact of anthropogenic land cover change on climate, *J. Clim.*, *20*(14), 3621–3634, doi:10.1175/JCLI4185.1.

Fischer, E. M., K. W. Oleson, and D. M. Lawrence (2012), Contrasting urban and rural heat stress responses to climate change, *Geophys. Res. Lett.*, *39*, L03705, doi:10.1029/2011GL050576.

GAMDT (2004), The new GFDL Global Atmosphere and Land Model AM2–LM2: Evaluation with prescribed SST simulations, *J. Clim.*, *17*(24), 4641–4673, doi:10.1175/JCLI-3223.1.

Grimmond, C. S. B. (1992), The suburban energy-balance––Methodological considerations and results for a midlatitude west-coast city under winter and spring conditions, *Int. J. Climatol.*, *12*(5), 481–497.

Grimmond, C. S. B. (2007), Urbanization and global environmental change: Local effects of urban warming, *Geogr. J.*, *173*, 83–88, doi:10.1111/j.1475-4959.2007.232_3.x.

Grimmond, C. S. B., J. A. Salmond, T. R. Oke, B. Offerle, and A. Lemonsu (2004), Flux and turbulence measurements at a densely built-up site in Marseille: Heat, mass (water and carbon dioxide), and momentum, *J. Geophys. Res.*, *109*, D24101, doi:10.1029/2004JD004936.

Grimmond, C. S. B., et al. (2010), The international urban energy balance models comparison project: First results from Phase 1, *J. Appl. Meteorol. Climatol.*, *49*(6), 1268–1292, doi:10.1175/2010jamc2354.1.

Grimmond, C. S. B., et al. (2011), Initial results from Phase 2 of the international urban energy balance model comparison, *Int. J. Climatol.*, *31*(2), 244–272, doi:10.1002/joc.2227.

Hamdi, R., and G. Schayes (2007), Validation of Martilli's urban boundary layer scheme with measurements from two mid-latitude European cities, *Atmos. Chem. Phys.*, *7*(17), 4513–4526.

Harman, I. N., M. J. Best, and S. E. Belcher (2004), Radiative exchange in an urban street canyon, *Boundary Layer Meteorol.*, *110*(2), 301–316, doi:10.1023/A:1026029822517.
Hurtt, G. C., et al. (2011), Harmonization of land-use scenarios for the period 1500–2100: 600 years of global gridded annual land-use transitions, wood harvest, and resulting secondary lands, *Clim. Change*, *109*(1–2), 117–161, doi:10.1007/s10584-011-0153-2.
Jackson, T. L., J. J. Feddema, K. W. Oleson, G. B. Bonan, and J. T. Bauerc (2010), Parameterization of urban characteristics for global climate modeling, Ann. *Assoc. Am. Geogr.*, *100*(4), 848–865.
Jarvi, L., C. S. B. Grimmond, and A. Christen (2011), The Surface Urban Energy and Water Balance Scheme (SUEWS): Evaluation in Los Angeles and Vancouver, *J. Hydrol.*, *411*(3-4), 219–237.
Jarvi, L., C. S. B. Grimmond, M. Taka, A. Nordbo, H. Setala, and I. B. Strachan (2014), Development of the Surface Urban Energy and Water Balance Scheme (SUEWS) for cold climate cities, *Geosci. Model. Dev.*, *7*(4), 1691–1711.
Kondo, H., Y. Genchi, Y. Kikegawa, Y. Ohashi, H. Yoshikado, and H. Komiyama (2005), Development of a multi-layer urban canopy model for the analysis of energy consumption in a big city: Structure of the urban canopy model and its basic performance, *Boundary Layer Meteorol.*, *116*(3), 395–421.
Kusaka, H., H. Kondo, Y. Kikegawa, and F. Kimura (2001), A simple single-layer urban canopy model for atmospheric models: Comparison with multi-layer and slab models, *Boundary Layer Meteorol.*, *101*(3), 329–358, doi:10.1023/A:1019207923078.
Lawrence, D. M., K. W. Oleson, M. G. Flanner, C. G. Fletcher, P. J. Lawrence, S. Levis, S. C. Swenson, and G. B. Bonan (2012), The CCSM4 Land Simulation, 1850-2005: Assessment of surface climate and new capabilities, *J. Clim.*, *25*(7), 2240–2260.
Lee, S. H., S. W. Kim, W. M. Angevine, L. Bianco, S. A. McKeen, C. J. Senff, M. Trainer, S. C. Tucker, and R. J. Zamora (2011), Evaluation of urban surface parameterizations in the WRF model using measurements during the Texas Air Quality Study 2006 field campaign, *Atmos. Chem. Phys.*, *11*(5), 2127–2143, doi:10.5194/acp-11-2127-2011.
Lemonsu, A., C. S. B. Grimmond, and V. Masson (2004), Modeling the surface energy balance of the core of an old Mediterranean city: Marseille, *J. Appl. Meteorol.*, *43*(2), 312–327.
Lemonsu, A., V. Masson, L. Shashua-Bar, E. Erell, and D. Pearlmutter (2012), Inclusion of vegetation in the Town Energy Balance model for modelling urban green areas, *Geosci. Model. Dev.*, *5*(6), 1377–1393, doi:10.5194/gmd-5-1377-2012.
Li, D., and E. Bou-Zeid (2013), Synergistic interactions between urban heat islands and heat waves: The impact in cities is larger than the sum of its parts, *J. Appl. Meteorol. Climatol.*, *52*(9), 2051–2064, doi:10.1175/JAMC-D-13-02.1.
Li, D., and E. Bou-Zeid (2014), Quality and sensitivity of high-resolution numerical simulation of urban heat islands, *Environ. Res. Lett.*, *9*(5), 055001.
Li, D., E. Bou-Zeid, M. L. Baeck, S. Jessup, and J. A. Smith (2013), Modeling land surface processes and heavy rainfall in urban environments: Sensitivity to urban surface representations, *J. Hydrometeorol.*, *14*(4), 1098–1118, doi:10.1175/jhm-d-12-0154.1.
Li, D., E. Bou-Zeid, and M. Oppenheimer (2014), The effectiveness of cool and green roofs as urban heat island mitigation strategies, *Environ. Res. Lett.*, *9*(5), 055002.
Li, D., T. Sun, M. F. Liu, L. Yang, L. Wang, and Z. Q. Gao (2015), Contrasting responses of urban and rural surface energy budgets to heat waves explain synergies between urban heat islands and heat waves, *Environ. Res. Lett.*, *10*(5), 054009.
MacDonald, R. W., R. F. Griffiths, and D. J. Hall (1998), An improved method for the estimation of surface roughness of obstacle arrays, *Atmos. Environ.*, *32*(11), 1857–1864, doi:10.1016/S1352-2310(97)00403-2.
Mahmood, R., et al. (2014), Land cover changes and their biogeophysical effects on climate, *Int. J. Climatol.*, *34*(4), 929–953, doi:10.1002/joc.3736.
Malyshev, S., E. Shevliakova, R. J. Stouffer, and S. W. Pacala (2015), Contrasting local vs. regional effects of land-use-change induced heterogeneity on historical climate: Analysis with the GFDL Earth System Model, *J. Clim.*, *28*(13), 5448–5469, doi:10.1175/JCLI-D-14-00586.1.
Martilli, A., A. Clappier, and M. W. Rotach (2002), An urban surface exchange parameterisation for mesoscale models, *Boundary Layer Meteorol.*, *104*(2), 261–304.
Masson, V. (2000), A physically-based scheme for the urban energy budget in atmospheric models, *Boundary Layer Meteorol.*, *94*(3), 357–397, doi:10.1023/A:1002463829265.
Masson, V. (2006), Urban surface modeling and the meso-scale impact of cities, *Theor. Appl. Climatol.*, *84*(1-3), 35–45, doi:10.1007/S00704-005-0142-3.
McCarthy, M. P., M. J. Best, and R. A. Betts (2010), Climate change in cities due to global warming and urban effects, *Geophys. Res. Lett.*, *37*, L09705, doi:10.1029/2010GL042845.
Mestayer, P. G., et al. (2005), The urban boundary-layer field campaign in Marseille (UBL/CLU-ESCOMPTE): Set-up and first results, *Boundary Layer Meteorol.*, *114*(2), 315–365.
Milly, P. C. D., S. L. Malyshev, E. Shevliakova, K. A. Dunne, K. L. Findell, T. Gleeson, Z. Liang, P. Phillipps, R. J. Stouffer, and S. Swenson (2014), An enhanced model of land water and energy for global hydrologic and earth-system studies, *J. Hydrometeorol.*, *15*(5), 1739–1761, doi:10.1175/JHM-D-13-0162.1.
Nie, W. S., T. Sun, and G. H. Ni (2014), Spatiotemporal characteristics of anthropogenic heat in an urban environment: A case study of Tsinghua Campus, *Building Environ.*, *82*, 675–686.
Niyogi, D., P. Pyle, M. Lei, S. P. Arya, C. M. Kishtawal, M. Shepherd, F. Chen, and B. Wolfe (2011), Urban modification of thunderstorms: An observational storm climatology and model case study for the Indianapolis Urban Region, *J. Appl. Meteorol. Climatol.*, *50*(5), 1129–1144, doi:10.1175/2010jamc1836.1.
Oke, T. R. (1982), The energetic basis of the urban heat-island, *Q. J. R. Meteorol. Soc.*, *108*(455), 1–24, doi:10.1002/qj.49710845502.
Oleson, K. W. (2012), Contrasts between urban and rural climate in CCSM4 CMIP5 climate change scenarios, *J. Clim.*, *25*(5), 1390–1412, doi:10.1175/JCLI-D-11-00098.1.
Oleson, K. W., G. B. Bonan, J. Feddema, M. Vertenstein, and C. S. B. Grimmond (2008), An urban parameterization for a global climate model. Part I: Formulation and evaluation for two cities, *J. Appl. Meteorol. Climatol.*, *47*(4), 1038–1060, doi:10.1175/2007JAMC1597.1.
Oleson, K. W., G. B. Bonan, J. Feddema, and T. Jackson (2011), An examination of urban heat island characteristics in a global climate model, *Int. J. Climatol.*, *31*(12), 1848–1865, doi:10.1002/joc.2201.
Pielke, R. A., et al. (2011), Land use/land cover changes and climate: Modeling analysis and observational evidence, *Wires Clim. Change*, *2*(6), 828–850, doi:10.1002/wcc.144.
Ramamurthy, P., and E. Bou-Zeid (2014), Contribution of impervious surfaces to urban evaporation, *Water Resour. Res.*, *50*, 2889–2902, doi:10.1002/2013WR013909.
Ramamurthy, P., E. Bou-Zeid, J. A. Smith, Z. H. Wang, M. L. Baeck, N. Z. Saliendra, J. L. Hom, and C. Welty (2014), Influence of subfacet heterogeneity and material properties on the urban surface energy budget, *J. Appl. Meteorol. Climatol.*, *53*(9), 2114–2129.
Rotach, M. W., et al. (2005), BUBBLE––An urban boundary layer meteorology project, *Theor. Appl. Climatol.*, *81*(3-4), 231–261, doi:10.1007/s00704-004-0117-9.

Ryu, Y. H., J. J. Baik, and S. H. Lee (2011), A new single-layer urban canopy model for use in mesoscale atmospheric models, *J. Appl. Meteorol. Climatol.*, *50*(9), 1773–1794.

Sailor, D. J. (2011), A review of methods for estimating anthropogenic heat and moisture emissions in the urban environment, *Int. J. Climatol.*, *31*(2), 189–199.

Sheffield, J., G. Goteti, and E. F. Wood (2006), Development of a 50-year high-resolution global dataset of meteorological forcings for land surface modeling, *J. Clim.*, *19*(13), 3088–3111.

Shepherd, J. M. (2005), A review of current investigations of urban-induced rainfall and recommmendations for the future, *Earth Interact.*, *9*, 1–27, doi:10.1175/EI156.1.

Shevliakova, E., S. W. Pacala, S. Malyshev, G. C. Hurtt, P. C. D. Milly, J. P. Caspersen, L. T. Sentman, J. P. Fisk, C. Wirth, and C. Crevoisier (2009), Carbon cycling under 300 years of land use change: Importance of the secondary vegetation sink, *Global Biogeochem. Cycles*, *23*, GB2022, doi:10.1029/2007GB003176.

Wang, L. L., D. Li, Z. Q. Gao, T. Sun, X. F. Guo, and E. Bou-Zeid (2014), Turbulent Transport of Momentum and Scalars Above an Urban Canopy, *Boundary Layer Meteorol.*, *150*(3), 485–511, doi:10.1007/S10546-013-9877-Z.

Wang, Z. H., E. Bou-Zeid, and J. A. Smith (2013), A coupled energy transport and hydrological model for urban canopies evaluated using a wireless sensor network, *Q. J. R. Meteorol. Soc.*, *139*(675), 1643–1657, doi:10.1002/qj.2032.

Wood, C. R., A. Lacser, J. F. Barlow, A. Padhra, S. E. Belcher, E. Nemitz, C. Helfter, D. Famulari, and C. S. B. Grimmond (2010), Turbulent flow at 190 m height above london during 2006-2008: A climatology and the applicability of similarity theory, *Boundary Layer Meteorol.*, *137*(1), 77–96, doi:10.1007/s10546-010-9516-x.

Yu, M., Y. M. Liu, Y. F. Dai, and A. Q. Yang (2013), Impact of urbanization on boundary layer structure in Beijing, *Clim. Change*, *120*(1-2), 123–136.

Zhang, D. L., Y. X. Shou, R. R. Dickerson, and F. Chen (2011), Impact of upstream urbanization on the urban heat island effects along the Washington-Baltimore Corridor, *J. Appl. Meteorol. Climatol.*, *50*(10), 2012–2029, doi:10.1175/JAMC-D-10-05008.1.